GEOPHYSICAL RESEARCH LETTERS, VOL. 22, NO. 9, PAGES 1037-1040, MAY 1, 1995

Estimation of an earthquake focal mechanism from a satellite radar interferogram: Application to the December 4, 1992 Landers aftershock

Kurt L. Feigl, Arnaud Sergent, and Dominique Jacq
Centre National de la Recherche Scientifique, Toulouse, France

Abstract. Using the interferometric fringes generated by the phase difference between a pair of synthetic-aperture radar (SAR) images acquired by the ERS-1 satellite, we estimate the focal mechanism of a small, shallow thrust earthquake. The inversion procedure is an iterative, linearized least-squares algorithm based on a standard elastic dislocation formulation for coseismic displacements. Our preferred estimate is a thrust focal mechanism with its hypocenter at (N34.35° ± 0.4 km, W116.91° ± 0.2 km, 2.6 ± 0.3 km depth) on a plane dipping southward beneath the San Bernardino Mountains, with a moment magnitude (M_W) of 5.4. The strike, dip, and rake are N106°E ± 7°, 28° ± 4°, and 93° ± 4°, respectively on a fault 3.1 ± 0.5 km wide and 2.9 ± 0.4 km long. The precision of these estimates is competitive with seismological determinations.

Introduction

Geodetic measurements of the coseismic deformation associated with shallow earthquakes are useful for determining the spatial extent of rupture on the fault plane. Because geodetic measurements are required both before and after the earthquake, however, the displacement field is spatially undersampled. The new technique of satellite radar interferometry can overcome this problem by providing dense spatial sampling in two dimensions with one measurement roughly every 100 m. This technique saw its first seismological application in the magnitude (M_W) 7.3 Landers earthquake of June 28, 1992, which generated over 7 m of displacement at the surface [*Massonnet et al.*, 1993; *Massonnet et al.*, 1994; *Zebker et al.*, 1994]. It is also capable of measuring much smaller earthquakes, such as the M_W = 5.1 aftershock of December 4, 1992 (Figure 1). The decimeter-sized displacement produced by this aftershock was well sampled by the radar aboard the ERS-1 satellite, but was not measured by any other geodetic technique. In this paper, we model the coseismic displacement field of the December 4 aftershock as recorded in the radar interferogram.

To measure the deformation, we analyze interference patterns constructed from the difference of two synthetic aperture radar (SAR) images acquired by the ERS-1 satellite. The resulting interferogram is a contour map of the change in range, that is, the component of the displacement vector which points toward the satellite. The details of the techniques used to calculate the interferograms are described elsewhere [*Massonnet and Rabaute*, 1993; *Massonnet et al.*, 1993; *Massonnet et al.*, 1994].

Paper number 94GL03212
0094-8534/95/94GL-03212$03.00

The ERS-1 satellite acquired one radar image of the epicentral area prior to the main June 28 shock at Landers, and eight afterward. The first coseismic interferogram, constructed from images acquired on April 24 and August 7, 1992, has been published previously [*Massonnet et al.*, 1993]. Taking the date of the main shock on June 28, 1992 as a temporal origin, we denote this interval of time as [–65,+40] days. Subsequent interferograms spanning different portions of the postseismic period covering the intervals [–65,+355], [+5,+180], and [+40, +355] d have been published as Figures 2a, b, and c, respectively in *Massonnet et al.* [1994].

The clearest observation of the displacement produced by the December 4 aftershock occurs in the interferogram for the interval [–65,+355] d. The fundamental observation consists of several round fringes centered on a point less than 2 km from the epicenter estimated from regional seismograms [*Hauksson et al.*, 1993]. The location of the earthquake is the first piece of evidence that it is responsible for the observed fringes.

The second piece of evidence is the date. The fringes are visible in the interferograms for the intervals [–65,+355], [+5,+180], and [+40, +355] d, but not in the interval [-65,+40] days [*Massonnet et al.*, 1994]. By elimination, the event which produced these fringes must have occurred in the interval [+40,+180] d, that is, between August 7 and December 25, 1992.

The third piece of evidence is the focal mechanism. Unlike most of the other Landers aftershocks with M_L magnitude greater than 5, the December 4 aftershock at 02:08 GMT has a thrust mechanism [*Hauksson et al.*, 1993; *Jones and Hough*, 1994]. Such a mechanism creates predominantly vertical displacements at the surface, which are more readily detected by radar than horizontal displacements. This is a geometric consequence of the 23° angle of incidence used by the ERS-1 radar.

The fourth piece of evidence is the shallow hypocentral depth of 2 km estimated from the seismological data [*Hauksson et al.*, 1993], which creates larger displacements at the surface than deeper events of the same magnitude. From the four pieces of evidence, we conclude that the December 4 aftershock generated the observed fringes because it is the only thrusting aftershock in the catalog with $M_L > 5$ and depth < 5 km to occur at the right place and the right time [*Hauksson et al.*, 1993].

Having identified the cause of the fringes, we next convert them from cycles of ambiguous phase into millimeters of absolute range change by counting and digitizing them (Figure 2). Because the digitized interferogram also contains fringes due to the Landers and Big Bear earthquakes, we subtract the range changes predicted by a model for these two events estimated from GPS measurements of coseismic displacement [*Hudnut et al.*, 1994]. This correction may be visualized as a sloping surface which is almost planar because the study area

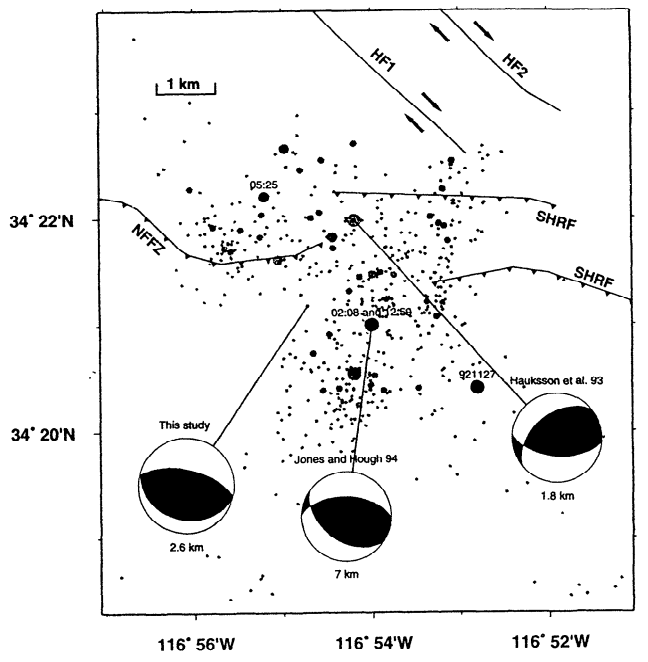

Figure 1. Location map showing faults with Holocene rupture: North Frontal Fault Zone (NFFZ), Sky High Ranch Fault (SHRF), and Helendale Fault (HF2); as well as a strand of the Helendale Fault (HF1) with Quaternary activity [*California Division of Mines and Geology*, 1992]. Three estimates of the focal mechanism of the 02:08 December 4, 1992 earthquake are also shown with depths and references. The epicenters of aftershocks recorded between June 27 and December 31, 1992 are shown with gray spots with diameter proportional to magnitude [*Hauksson et al.*, 1993]. Black dots denote epicenters estimated by *Jones and Hough* [1994] for events at 05:25 GMT (M_w = 4.3), at 12:59 (M_w = 4.2), and on November 27 (M_w = 5.1).

is over 50 km from the Landers mainshock epicenter. The same model is used to identify the fringe corresponding to zero deformation, that is, the contour corresponding to the position of the ground surface prior to the Landers earthquake sequence. The result is a data set consisting of the range component of coseismic displacement measured at 477 points. These changes in range are assumed to have been produced primarily by the M_W = 5.1 aftershock at 02:08 GMT on December 4. Three other events may also make a small contribution to the range change: a M_W = 4.2 aftershock at 12:59 GMT at the same location but at 8 km depth, a M_W = 4.3 aftershock at 05:25 GMT at 5 km depth several km to the NW, and a M_W = 5.1 strike-slip event on November 27 at 5 km depth several km to the SE (solid dots in Figure 1)[*Jones and Hough*, 1994].

Inverse problem

Given the observed range changes, we seek the earthquake source parameters $\mathbf{p}$ which best fit these data $\mathbf{d}$. The relation $\mathbf{d} = \mathbf{g}(\mathbf{p})$ is assumed to be the result of a dislocation on a rectangular fault buried in an elastic half space [*Okada*, 1985]. The two Lamé moduli, λ and μ, are taken to be equal to approximate the crust as a Poisson solid. Using this description, the surface displacement vector $\mathbf{u}$ can be calculated from ten parameters $\mathbf{p} = [X, Y, d, \alpha, \delta, L, W, U_1, U_2, U_3]$, where X, Y, and d give the east, north, and vertical coordinates of the lower left-hand corner of the rectangular fault patch in km; α and d its strike and dip in degrees; L and W its length and width in km. The triplet (U_1, U_2, U_3) gives the left-lateral, up-dip, and tensile components of the fault slip vector $\mathbf{U}$ in mm. Following this calculation, the scalar change in range is calculated $\Delta\rho = -\mathbf{u} \cdot \hat{\mathbf{s}}$, where $\hat{\mathbf{s}}$ is the unit vector pointing from the ground point toward the satellite.

The inverse problem consists of minimizing the difference between the observed range change $\mathbf{d}$ and the modeled range change $\mathbf{g}(\mathbf{p})$. It can be solved using an iterative linearized least-squares scheme since the function $\mathbf{g}$ is not sharply nonlinear and we have a reasonable prior model $\mathbf{p_0}$ from the seismological focal mechanism. Specifically, we use equation (25) of *Tarantola and Valette* [1982], with diagonal matrices for the data covariance $\mathbf{C}_{d_0 d_0}$ and the prior model covariance $\mathbf{C}_{p_0 p_0}$. The standard deviation for each data point is assumed to be 34 mm in range, based on a comparison with GPS measurements of the coseismic displacements at Landers [*Massonnet et al.*, 1993]. For the model covariance, we have assumed reasonably loose values, such that the square roots of the diagonal elements of $\mathbf{C}_{p_0 p_0}$ are 1 km for X, Y, d, L, and W; 10° for α and δ; 100 mm for U_1 and U_2; 0.01 mm for U_3. The tight constraint on the tensile component U_3 restricts the solution to a double-couple mechanism.

We begin with a prior model $\mathbf{p_0}$ in which X, Y, d, α and δ are taken from the seismological estimate [*Hauksson et al.*, 1993] and U_1 = 112 mm, U_2 = 195 mm, U_3 = 0 mm,

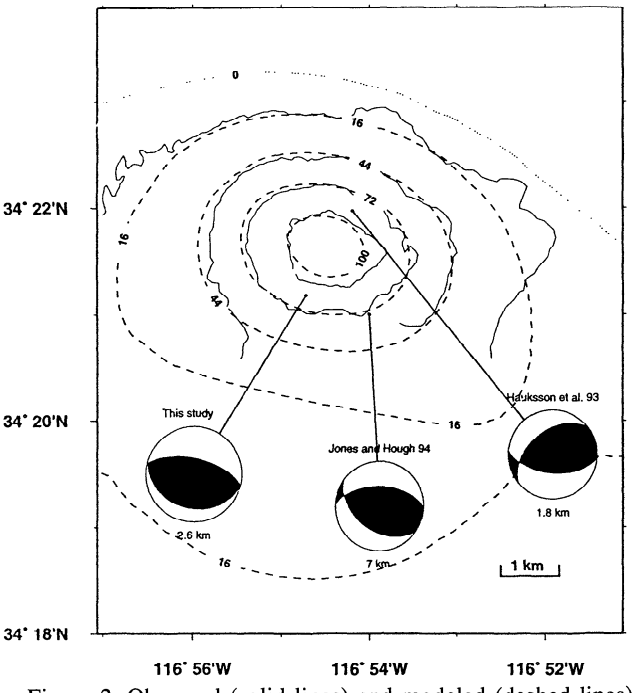

Figure 2. Observed (solid lines) and modeled (dashed lines) values of the range component of uplift in mm. The observed values were obtained by digitizing a subset of an interferogram formed from SAR images acquired by the ERS-1 satellite on April 24, 1992 and June 18, 1993, as published in Figure 3b of [*Massonnet et al.*, 1994]. The contour of zero deformation has been chosen to correspond to the topographic surface prior to the Landers mainshock, as identified from the synthetic fringes calculated from an independent model for the Landers sequence [*Hudnut et al.*, 1994].

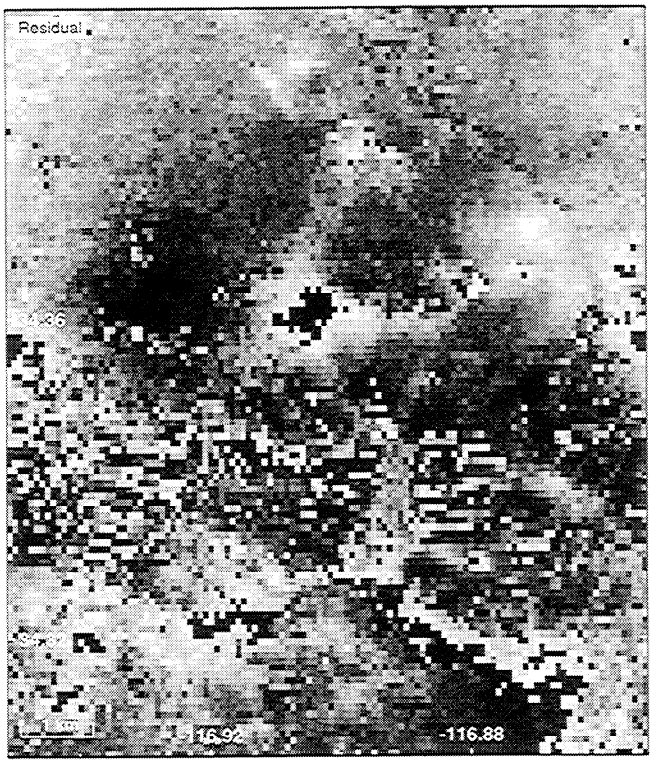

Figure 3. Residual interference pattern generated by subtracting synthetic fringes from the observed interferogram using modular arithmetic. Less than one cycle (28 mm) of unmodeled deformation remains.

L = 2.5 km, and W = 2.4 km were chosen to provide a moment of $\mu ULW = 4.3 \times 10^{16}$ N.m, or M_W = 5.1. (Here, and in the rest of this paper, we take the shear modulus μ to be 32 GPa.) This fault model, which we call "model A", does not fit the data particularly well, since the RMS of the difference $\mathbf{d} - \mathbf{g}(\mathbf{p_A})$ is 41 mm, somewhat larger than the 34 mm assumed for the accuracy of the radar measurements. Indeed, this model is sufficiently far from the optimal solution that the iterative estimation scheme does not converge. Apparently, the linearization of the function $\mathbf{g}$ is not valid in this portion of the model space.

To avoid this difficulty, we revert to forward modeling by trial and error. By generating synthetic fringes from different sets of fault parameters and comparing them with the observed fringes, it is relatively easy to find an acceptable new model ("B"). The misfit of model B, as measured by the RMS of the difference $\mathbf{d} - \mathbf{g}(\mathbf{p_B})$, is only 17 mm, better than model A by a factor of 2.4. In performing this exercise, we find that the fringes in the synthetic interferogram are particularly sensitive to the strike and depth of the fault patch.

Using model B as a prior model in the iterative least-squares inversion algorithm, we reach convergence within five iterations. The result, called model C, has an RMS misfit of 4.7 mm, better than model A by a factor of 8. It predicts interferometric fringes which are quite close to those in the observed interferogram (Figure 2). The residual interferogram (Figure 3), is obtained by subtracting the synthetic fringes from the observed fringes using a modulo operator which preserves the cyclic nature of the interferometric phase. The RMS scatter in this residual is 0.4 cycle, or 12 mm, about twice as high as the misfit determined from the 477 points alone. The good fit of the model to a superset of the data used to estimate it confirms that very little deformation remains unmodeled in the interferogram. It also suggests that the a priori value of 34 mm overestimates the uncertainty in the radar measurements of range change. This may reflect tropospheric errors in the vertical component of the GPS estimates used for the calibration. In this case, the actual uncertainty in the radar range would be better described by the 4 mm value predicted by propagating the topographic error into this interferogram [*Massonnet et al.*, 1994]. Thus, the topographic error inherited from the digital elevation model appears to be the dominant source of uncertainty in the interferogram at short spatial scales.

The a posteriori uncertainty associated with each parameter estimate is calculated by Monte Carlo simulation. We add normally distributed, random perturbations to the data based on the a priori standard deviation of 34 mm. When inverted, the perturbed data yield a family of parameter estimates, for which the sample variance measures the a posteriori variance of model C. The square root of this quantity gives a posteriori uncertainty σ listed in Table 1. In performing these calculations, we effectively explore the model space in the neighborhood of model C, but do not find any other nearby (local) minima in misfit.

To evaluate the resolution, we consider the ratio of the a priori uncertainty to the a posteriori uncertainty for each parameter. This ratio is greater than 2 for all parameters except the strike α, for which the value is only 1.4, indicating poor resolution of this parameter.

Table 1. Focal Mechanism Parameters for Event at 02:08 GMT on December 4, 1992

Model	longitude*	latitude*	depth* km	strike deg. CW	dip deg.	rake deg. CCW	U_1 mm	U_2 mm	U_3 mm	L km	W km	M_w
Hauksson *et al.* [1993]	W116.90°	N34.37°	1.8	95	55	120						5.1
Jones and Hough [1994]	W116.90°	N34.35°	7	126	43	117						5.1
This study	W116.91°	N34.35°	2.6	106	28	93	–22	514	0	2.9	3.1	5.4
Hauksson *et al.* σ	1 km	1 km	1	10	24	25						
A priori σ	1 km	1 km	1	10	10		100	100	0.01	1	1	0.3
A posteriori σ	0.2 km	0.4 km	0.3	7	3.5	4	40	37		0.4	0.5	0.1
Prior/post	4.8	2.5	3.3	1.4	2.8		2.5	2.7		2.8	2.1	3.4

* Coordinates of hypocenter at the center of a rectangular fault

Interpretation

The radar estimate agrees with two seismological estimates [*Hauksson et al.*, 1993; *Jones and Hough*, 1994] for all parameters except depth and magnitude (Figure 1 and Table 1). The radar estimate of the epicentral location is less than 2.5 km from either seismological estimate, within the 2-dimensional 95% (2.45 σ) confidence ellipse if the average 1 km uncertainty given for the entire catalog in the former study is applicable. The radar estimate of the hypocentral depth 2.6 ± 0.3 km agrees with the 1.8 ± 1.0 km provided by the seismological catalog [*Hauksson et al.*, 1993] but not with the 7 km value obtained by a grid search [*Jones and Hough*, 1994]. We note, however, that the latter algorithm uncovered a secondary minimum at 2 km depth with an indistinguishable mechanism (L. E. Jones, pers. comm., 1994).

The radar inversion procedure yields a thrusting focal mechanism which resembles the seismological estimates obtained using the standard HYPOINVERSE procedure [*Hauksson et al.*, 1993] and a grid-search scheme [*Jones and Hough*, 1994]. The uncertainties in the former study are 10°, 24°, and 25° for strike, dip, and rake, respectively, on average for the entire catalog. The radar estimates fall within the 95% (1.96 σ) confidence limits for these parameters. The a posteriori uncertainties for the radar estimates are 7°, 3.5° and 4° for strike, dip and rake, respectively.

For the moment magnitude M_W, the radar estimate is 5.4 ± 0.1, significantly larger than the value of 5.1 estimated from the two seismological studies. The usual explanation for such a difference in magnitude is that not all the strain energy released as permanent deformation is radiated as seismic waves. A more likely explanation is that the interferogram includes deformation produced by more than one earthquake. The three events noted earlier (05:25, 12:59, and 921127 in Figure 1) probably also contribute to the surface deformation recorded by the interferogram. The contribution is small, however, because all three of these events occurred below 5 km depth, almost twice the depth estimated by radar for the 02:08 event. Adding the moments for these three events to the seismological estimate for the 02:08 earthquake yields a total moment release equivalent to $M_W = 5.3$. In this sense, the radar estimate represents a composite mechanism for the ensemble of shallow earthquakes in this area between August 7 and December 25, 1992.

Throughout our analysis, we have assumed that the south-dipping focal plane is the rupture plane. This assumption is consistent with the southward dip of the North Frontal Fault Zone (NFFZ) and Sky Hi Ranch fault (SHRF) which bound the range front of the San Bernardino Mountains by dipping below them [*Meisling and Weldon*, 1989]. The south-dipping plane is also partially favored by the observation that most of the small aftershocks in the area occur to the south of the surface trace of the NFFZ and SHRF (Figure 1). On the other hand, the possibility of a north-dipping fault plane cannot be excluded solely on the basis of the radar data. Not surprisingly, there exists another local minimum in the surface of data-model misfit. This second possible solution indicates a north-dipping focal plane with essentially the same geometry as our preferred south-dipping solution, but with an epicenter several kilometers to the north. The RMS misfit of this solution, is 5.1 mm, not distinguishably different from the 4.7 mm for the preferred south-dipping solution. Despite the high spatial sampling of the radar data, they are apparently insufficient to resolve the difference between the two fault planes in a double couple. We note, of course, that these differences arise only from the finite extent of the fault plane used in our model. These differences are not especially noticeable for the December 4 earthquake because the fault patch is almost square.

By using a radar interferogram acquired by satellite, we have, for the first time, determined the focal mechanism of an earthquake without an instrument on the ground. The accuracy of the estimate surpasses similar geodetic procedures and rivals seismological approaches. Although the prerequisites for the radar technique are admittedly restrictive, its application could prove quite useful in remote areas without local seismographic networks, such as Asia, or, in principle, other planets.

Acknowledgments. We thank Didier Massonnet and his group at CNES for producing the interferogram. Egil Hauksson kindly provided focal mechanisms. Constructive comments from Laura Jones, Anne Briais, Annie Souriau, and two anonymous reviewers improved the manuscript. All figures were made with the public domain GMT software. This work was supported by a grant from PNTS 94, and CNES student internships for A.S. and D.J.

References

California Division of Mines and Geology, Preliminary fault activity map of California, Calif. Dept. of Conservation, Sacramento, 1992.

Hauksson, E., L. M. Jones, K. Hutton, and D. Eberhart-Phillips, The 1992 Landers earthquake sequence, *J. Geophys. Res.*, *98*, 19,835–19,858, 1993.

Hudnut, K. W. et al., Coseismic displacements of the 1992 Landers earthquake sequence, *Bull. Seism. Soc. Amer.*, *84*, 625–645, 1994.

Jones, L. E., and S. E. Hough, Analysis of broadband records from the June 28, 1992 Big Bear earthquake: evidence of a multiple-event source, *Bull. Seism. Soc. Amer.*, *in press*, 1994.

Massonnet, D., and T. Rabaute, Radar interferometry: limits and potential, *IEEE Trans. Geoscience & Rem. Sensing*, *31*, 455–464, 1993.

Massonnet, D., M. Rossi, C. Carmona, F. Adragna, G. Peltzer, K. Feigl, and T. Rabaute, The displacement field of the Landers earthquake mapped by radar interferometry, *Nature*, *364*, 138-142, 1993.

Massonnet, D., K. L. Feigl, M. Rossi, and F. Adragna, Radar interferometric mapping of deformation in the year after the Landers earthquake, *Nature*, *369*, 227–230, 1994.

Meisling, K. E., and R. J. Weldon, Late Cenozoic tectonics of the northwestern San Bernardino Mountains, southern California, *Geol. Soc. Amer. Bull.*, *101*, 106-128, 1989.

Okada, Y., Surface deformation to shear and tensile faults in a half-space, *Bull. Seism. Assoc. Amer.*, *75*, 1135-1154, 1985.

Zebker, H. A., P. A. Rosen, R. M. Goldstein, A. Gabriel, and C. L. Werner, On the derivation of coseismic displacement fields using differential radar interferometry: the Landers earthquake, *J. Geophys. Res.*, *99*, 19,617–19,634, 1994.

Kurt L. Feigl, Arnaud Sergent, and Dominique Jacq, CNRS UPR 234, Observatoire Midi-Pyrénées, 14 Avenue Edouard Belin, 31400 France. (e-mail: feigl@medoc.cnes.fr).

(Received: September 23, 1994; accepted October 26, 1994.)